Springer

KSME

Journal of Mechanical Science and Technology 26 (5) (2012) 1577~1583
www.springerlink.com/content/1738-494x
DOI 10.1007/s12206-012-0338-2

Frequency shift of a nanomechanical sensor carrying a nanoparticle using nonlocal Timoshenko beam theory †

Zhi-Bin Shen, Dao-Kui Li, Dong Li and Guo-Jin Tang*

College of Aerospace and Materials Engineering, National University of Defense Technology, Changsha, Hunan 410073, China

(Manuscript Received September 20, 2011; Revised January 14, 2012; Accepted January 18, 2012)

Abstract

The frequency shift of a nanomechanical sensor carrying a nanoparticle is studied. A bridged single-walled carbon nanotube (SWCNT) carrying a nanoparticle is modeled as a clamped micro-beam with a concentrated micro-mass at any position. Based on the nonlocal Timoshenko theory of beams, which incorporates size effects into the classical theory, the natural frequencies of the nanomechanical sensor are derived using the transfer function method. The effects of the mass and position of the nanoparticle on the frequency shift are discussed. In the absence of the nonlocal effect, the frequencies are reduced to the results of the classical model, in agreement with those using the finite element method. The obtained results show that when the mass of the attached nanoparticle increases or its location is close to the beam center, the natural frequency decreases, but the shift in frequency increases. The effect of the nonlocal parameter on the frequency shift is significant. Decreasing the length-to-diameter ratio also increases the frequency shift. The natural frequencies and shifts are strongly affected by rotary inertia, and the nonlocal Timoshenko beam model is more adequate than the nonlocal Euler-Bernoulli beam model for short nanomechanical sensors. The obtained results are helpful in the design of SWCNT-based resonator as nanomechanical mass sensor.

Keywords: SWCNT; Nanomechanical sensor; Nonlocal theory; Timoshenko beam; Transfer function method; Frequency shift

1. Introduction

Since the discovery of carbon nanotubes (CNTs) by Iijima [1] in 1991, they have demonstrated a significant potential for use in a diverse range of new and evolving applications [2-5]. Poncharal et al. [6] first proposed the idea of using individual CNTs as high sensitivity nanobalances in 1999. The extraordinary mechanical and physical properties, in addition to the large aspect ratio, low density, and high stiffness, make CNTs promising candidates for atomic-resolution mass sensors [7].

The nanosized mass sensor with a resonator is based on the fact that resonant frequency is sensitive to the attached mass [8]. The change of the attached mass and its location on the resonator causes a shift to the resonant frequency. To analyze the effects of the attached mass and its location on the resonant frequency of CNT-based nanomechanical sensors, the classical Euler-Bernoulli beam theory (EBT) has been used to model a nanomechanical resonator [8-10]. However, the effects of shear deformation and rotary inertia are neglected in previous analyses. When these two factors are taken into account simultaneously, the Timoshenko beam theory (TBT) [11] is necessary and also more effective. Some theoretical analyses involving wave propagation and free vibration of CNTs have also been presented [12-14] using the TBT.

In addition, classical continuum models are assumed to be scale-independent and cannot be used to describe the size effects arising from the small scale. The classical continuum theory, when applied to the analyses of nanostructures such as CNTs, is inadequate because it ignores the small scale effect. To improve this situation, the nonlocal elasticity theory presented by Eringen [15, 16] has been developed to tackle scale-dependent problems. Along this line, Lee et al. [17] used the nonlocal EBT to analyze the frequency shift of CNT-based mass sensors. However, shear deformation and rotary inertia have been neglected. To the best of the authors' knowledge, few research efforts treat the frequency shift of CNT-based nanomechanical mass sensors via the nonlocal TBT.

A nanomechanical sensor should simultaneously detect the mass and position of the attached nanoparticle. In the present study, the dynamic behavior of nanomechanical resonators as nanosized mass sensors is examined, and a clamped nonlocal Timoshenko beam with an attached nanoparticle is modeled. The transfer function method (TFM) [18-20] is used to determine the natural frequencies of the nanomechanical sensor. The frequency shift of a single-walled carbon nanotube (SWCNT)-

*Corresponding author. Tel.: +86 731 84573107, Fax.: +86 731 84512301
E-mail address: tanggj@nudt.edu.cn
† Recommended by Editor Maenghyo Cho.

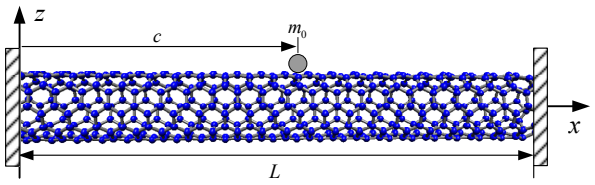

Fig. 1. Bridged SWCNT-based nanomechanical mass sensor with an attached nanoparticle.

based nanomechanical sensor with a nanoparticle is also studied. In addition, the effects of the nonlocal parameter, aspect ratio, rotary inertia, mass, and location of the nanoparticle on the frequency shift of the bridged SWCNT are analyzed.

2. Theoretical model

2.1 Dynamic equation of the SWCNT sensor based on nonlocal TBT

This study considers the bridged SWCNT-based nanomechanical sensor, which is one of two frequently-used CNT-based nanomechanical sensors [8, 21, 22]. To further simplify the model, which is similar to the conventional treatment as in [23, 24], the bridged SWCNT sensor is modeled as a clamped-clamped beam carrying a nanoparticle located at c from the left fixed end $x = 0$, as shown in Fig. 1. Attention is paid to the effects of the attached mass on the natural frequencies of the vibrating system.

As in the classical TBT, only two independent variables are considered: namely, the transverse displacement w and the rotation of cross-section θ, both of which depend on the longitudinal coordinate x and time t. According to Hamilton's principle and Eringen's nonlocal elasticity theory [15, 16], the governing equations of the nonlocal TBT can be expressed as [12, 25]

$$\rho A\left[1-(e_0a)^2\frac{\partial^2}{\partial x^2}\right]\frac{\partial^2 w}{\partial t^2}-\kappa GA\left(\frac{\partial\theta}{\partial x}+\frac{\partial^2 w}{\partial x^2}\right)=0 \tag{1}$$

$$\rho I\left[1-(e_0a)^2\frac{\partial^2}{\partial x^2}\right]\frac{\partial^2\theta}{\partial t^2}+\kappa GA\left(\theta+\frac{\partial w}{\partial x}\right)-EI\frac{\partial^2\theta}{\partial x^2}=0 \tag{2}$$

where ρ is the mass density; A and I are the cross-sectional area and its second moment, respectively; E and G are the Young's modulus and shear modulus, respectively. κ is the shear correction factor depending on the material and geometric parameters of the beam, which is introduced to account for the relaxation of the inconsistency of the usual shear-free boundary condition at the beam surface. e_0a is the small scale parameter with length unit which can be used to describe the size effects; e_0 is a nondimensional material constant that can be determined by experiments or numerical simulations from lattice dynamics, and a denotes the C–C bond length. The nonlocal effects are assumed to be present for both normal and shear stresses. When $e_0a = 0$, the nonlocal elasticity reduces to the classical TBT [11].

In addition, the nonlocal bending moment M and the nonlocal shearing force Q can be expressed as below, respectively,

$$M(x,t)=EI\frac{\partial\theta}{\partial x}+(e_0a)^2\left[\rho A\frac{\partial^2 w}{\partial t^2}+\rho I\frac{\partial^3\theta}{\partial x\partial t^2}\right] \tag{3}$$

$$Q(x,t)=\kappa GA\left(\theta+\frac{\partial w}{\partial x}\right)+(e_0a)^2\rho A\frac{\partial^3 w}{\partial x\partial t^2}. \tag{4}$$

For the bridged SWCNT, the corresponding boundary conditions read

$$w_1(0,t)=\theta_1(0,t)=w_2(L,t)=\theta_2(L,t)=0 \tag{5}$$

where w_1, w_2 and θ_1, θ_2 are the transverse displacements and cross-section rotation on two clamped ends, respectively. When a nanoparticle with mass m_0, such as a buckyball, molecule, or bacterium, is attached to location $x = c$, the compatibility conditions at the position of the attached mass must be satisfied, namely,

$$w_1(c,t)=w_2(c,t),\ \ \theta_1(c,t)=\theta_2(c,t) \tag{6}$$

$$M_1(c,t)=M_2(c,t) \tag{7}$$

$$Q_1(c,t)+m_o\frac{\partial^2 w_1(c,t)}{\partial t^2}=Q_2(c,t) \tag{8}$$

where M_i and Q_i are obtained by substituting w_i and θ_i into Eqs. (3) and (4) (i = 1,2). Subscripts 1 and 2 denote the quantities associated with the left and the right hand of the attached nanoparticle, respectively.

Furthermore, initial conditions can be assumed as

$$w_{1,2}(x,0)=\frac{\partial w_{1,2}(x,0)}{\partial t}=0 \tag{9}$$

$$\theta_{1,2}(x,0)=\frac{\partial\theta_{1,2}(x,0)}{\partial t}=0. \tag{10}$$

2.2 Special case: nonlocal EBT

Results for the nonlocal EBT can also be analytically derived from the above. Eliminating $\kappa GA\left(\frac{\partial\theta}{\partial x}+\frac{\partial^2 w}{\partial x^2}\right)$ from Eqs. (1) and (2) yields

$$EI\frac{\partial^3\theta}{\partial x^3}-\rho I\left[1-(e_0a)^2\frac{\partial^2}{\partial x^2}\right]\frac{\partial^3\theta}{\partial x\partial t^2}-\rho A\left[1-(e_0a)^2\frac{\partial^2}{\partial x^2}\right]\frac{\partial^2 w}{\partial t^2}=0. \tag{11}$$

The Euler-Bernoulli hypothesis neglects the effects of shear deformation and rotary inertia of the beam. The Euler-Bernoulli hypothesis is actually equivalent to a sufficiently large shear modulus or shear rigidity, which impedes shear deformation in the beam. Consequently, in the above formula-

tion, $\kappa GA/EI \to \infty$ and the influence of the rotary inertia, i.e., $\rho I\partial^2\theta/\partial t^2 = 0$, is neglected. Eq. (2) is reduced to

$$\theta = -\frac{\partial w}{\partial x}. \tag{12}$$

By setting $\rho I\partial^2\theta/\partial t^2 = 0$ and substituting Eq. (12) into Eq. (11), the governing equation of nonlocal EBT

$$EI\frac{\partial^4 w}{\partial x^4} + \rho A\left[1-(e_0a)^2\frac{\partial^2}{\partial x^2}\right]\frac{\partial^2 w}{\partial t^2} = 0 \tag{13}$$

is recovered [17]. Moreover, other physical quantities can be given in terms of w. That is,

$$M(x,t) = -EI\frac{\partial^2 w}{\partial x^2} + (e_0a)^2\rho A\frac{\partial^2 w}{\partial t^2} \tag{14}$$

$$Q(x,t) = -EI\frac{\partial^3 w}{\partial x^3} + (e_0a)^2\rho A\frac{\partial^3 w}{\partial x\partial t^2}. \tag{15}$$

In this case, the boundary conditions in (5), as well as the initial conditions in (9) and (10), are the same, whereas those in (7) and (8) should be replaced by

$$\left[-EI\frac{\partial^2}{\partial x^2} + (e_0a)^2\rho A\frac{\partial^2}{\partial t^2}\right][w_1(c,t) - w_2(c,t)] = 0 \tag{16}$$

$$\left[-EI\frac{\partial^3}{\partial x^3} + (e_0a)^2\rho A\frac{\partial^3 w}{\partial x\partial t^2}\right][w_1(c,t) - w_2(c,t)] + m_0\frac{\partial^2 w_1(c,t)}{\partial t^2} = 0. \tag{17}$$

3. Solution method

3.1 Nonlocal TBT

In solving for the free vibration of Timoshenko beams, the TFM, as a powerful semi-analytical and semi-numerical method, is frequently applied to treat relevant problems. For example, Adhikari et al. [26] presented a closed-form solution for a beam with nonlocal damping using the TFM for the distributed parameter system. In this section, the TFM is employed to investigate the free vibration of the SWCNT-based sensor.

With the aid of the initial conditions Eqs. (9) and (10), and after performing the Laplace transform, the governing Eqs. (1) and (2) can be written as follows:

$$\rho As^2\left[1-(e_0a)^2\frac{\partial^2}{\partial x^2}\right]\tilde{w} - \kappa GA\left(\frac{\partial\tilde{\theta}}{\partial x} + \frac{\partial^2\tilde{w}}{\partial x^2}\right) = 0 \tag{18}$$

$$\rho Is^2\left[1-(e_0a)^2\frac{\partial^2}{\partial x^2}\right]\tilde{\theta} + \kappa GA\left(\tilde{\theta} + \frac{\partial\tilde{w}}{\partial x}\right) - EI\frac{\partial^2\tilde{\theta}}{\partial x^2} = 0 \tag{19}$$

where $\tilde{w}$, $\tilde{\theta}$ are the Laplace transform form of w, θ, respectively, and s is the Laplace transform parameter.

By introducing the following nondimensional parameters, $X = x/L$, $W = w/L$, $\alpha = \frac{I}{AL^2}$, $\beta = \frac{EI}{\kappa GAL^2}$, $\Gamma = \frac{\rho AL^4}{EI}s^2$, and $\lambda = \frac{e_0a}{L}$, Eqs. (18) and (19) may be rewritten as

$$\frac{\partial^2\tilde{W}}{\partial X^2} = \frac{\Gamma\beta}{1+\Gamma\beta\lambda^2}\tilde{W} - \frac{1}{1+\Gamma\beta\lambda^2}\frac{\partial\tilde{\theta}}{\partial X} \tag{20}$$

$$\frac{\partial^2\tilde{\theta}}{\partial X^2} = \frac{1}{\beta(1+\Gamma\alpha\lambda^2)}\frac{\partial\tilde{W}}{\partial X} + \frac{1+\Gamma\alpha\beta}{\beta(1+\Gamma\alpha\lambda^2)}\tilde{\theta}. \tag{21}$$

If denoting a status vector as

$$\boldsymbol{\eta}(X,s) = [\tilde{W}_1, \frac{\partial\tilde{W}_1}{\partial X}, \tilde{\theta}_1, \frac{\partial\tilde{\theta}_1}{\partial X}, \tilde{W}_2, \frac{\partial\tilde{W}_2}{\partial X}, \tilde{\theta}_2, \frac{\partial\tilde{\theta}_2}{\partial X}]^{\mathrm{T}}$$

where the superscript T denotes matrix transpose, Eqs. (20) and (21) can be rewritten in a compact form in state space:

$$\frac{\mathrm{d}\boldsymbol{\eta}(X,s)}{\mathrm{d}X} = \boldsymbol{\Phi}(s)\boldsymbol{\eta}(X,s) + \mathbf{g}(X,s) \tag{22}$$

where $\boldsymbol{\Phi}(s) = [\Phi_{ij}]_{8\times8}$ is an 8×8 matrix with variable s, in which

$$\Phi_{21} = \Phi_{65} = \frac{\beta\Gamma}{1+\beta\Gamma\lambda^2},\quad \Phi_{24} = \Phi_{68} = \frac{-1}{1+\beta\Gamma\lambda^2},$$

$$\Phi_{42} = \Phi_{86} = \frac{1}{\beta(1+\beta\Gamma\lambda^2)},\quad \Phi_{43} = \Phi_{87} = \frac{\alpha\beta\Gamma+1}{\beta(1+\beta\Gamma\lambda^2)}$$

and other elements in $\boldsymbol{\Phi}(s)$ vanish. $\mathbf{g}(X,s)$ is related to the distributed loading and vanishes for the present study.

Next, after performing the Laplace transform to two sides of the boundary conditions (5) and the compatibility conditions (6) to (8), with the vanishing initial conditions, the results are shown below:

$$\tilde{W}_1(0,s) = \tilde{\theta}_1(0,s) = \tilde{W}_2(1,s) = \tilde{\theta}_2(1,s) = 0, \tag{23}$$

$$\tilde{W}_1(\delta,s) = \tilde{W}_2(\delta,s),\ \ \tilde{\theta}_1(\delta,s) = \tilde{\theta}_2(\delta,s), \tag{24}$$

$$\begin{aligned}&\Gamma\lambda^2\tilde{W}_1(\delta,s) + \left(1+\alpha\Gamma\lambda^2\right)\frac{\partial\tilde{\theta}_1(\delta,s)}{\partial X}\\ &-\Gamma\lambda^2\tilde{W}_2(\delta,s) - (1+\alpha\Gamma\lambda^2)\frac{\partial\tilde{\theta}_2(\delta,s)}{\partial X} = 0\end{aligned}, \tag{25}$$

$$\begin{aligned}&m\beta\Gamma\tilde{W}_1(\delta,s) + (1+\beta\Gamma\lambda^2)\frac{\partial\tilde{W}_1(\delta,s)}{\partial X}\\ &-(1+\beta\Gamma\lambda^2)\frac{\partial\tilde{W}_2(\delta,s)}{\partial X} + \tilde{\theta}_1 - \tilde{\theta}_2 = 0\end{aligned}, \tag{26}$$

where $m = m_0/\rho AL$ and $\delta = c/L$ are the nondimensional mass and position of the attached nanoparticle, respectively. Furthermore, using the introduced vector $\boldsymbol{\eta}$, Eqs. (23) to (26) can be rewritten as

$$\mathbf{M}_{\mathrm{b}}\boldsymbol{\eta}(0,s) + \mathbf{N}_{\mathrm{b}}\boldsymbol{\eta}(1,s) + \mathbf{R}_c(s)\boldsymbol{\eta}(\delta,s) = \boldsymbol{\gamma}(s) \tag{27}$$

where $\mathbf{M}_{\mathrm{b}}=[M_{ij}]_{8\times8}$, $\mathbf{N}_{\mathrm{b}}=[N_{ij}]_{8\times8}$, and $\mathbf{R}_{\mathrm{c}}=[R_{ij}]_{8\times8}$ are 8×8 matrices, in which

$$M_{11}=M_{23}=1,\ N_{35}=N_{47}=1,\ R_{51}=R_{63}=R_{83}=1,$$
$$R_{55}=R_{67}=R_{87}=-1,\ R_{71}=-R_{75}=\Gamma\lambda^2,$$
$$R_{74}=-R_{78}=1+\alpha\Gamma\lambda^2,\ R_{81}=m\beta\Gamma,$$
$$R_{82}=-R_{86}=1+\beta\Gamma\lambda^2$$

and other elements in $\mathbf{M}_b$, $\mathbf{N}_b$ and $\mathbf{R}_c$ vanish. $\boldsymbol{\gamma}(s)$ in Eq. (27) is a vector determined by the force or displacement in the end. $\boldsymbol{\gamma}(s)=0$ can be found easily.

According to the TFM, the solution to Eq. (22) can be expressed as follows [20]:

$$\begin{aligned}&\left[\mathbf{M}_{\mathrm{b}}+\mathbf{N}_{\mathrm{b}}e^{\boldsymbol{\Phi}(s)}+\mathbf{R}_c(s)\mathrm{e}^{\boldsymbol{\Phi}(s)\delta}\right]\boldsymbol{\eta}(X,s)\\&=\int_0^{\mathrm{L}}\mathbf{G}(X,\xi,s)\mathbf{g}(\xi,s)\mathrm{d}\xi+\mathrm{e}^{\boldsymbol{\Phi}(s)X}\gamma(s)\end{aligned}\tag{28}$$

where

$$\mathbf{G}(X,\xi,s)=\begin{cases}\mathbf{M}_{\mathrm{b}}\mathrm{e}^{-\boldsymbol{\Phi}(s)\xi} & \mathrm{X}\geq\xi\\ -\mathbf{N}_{\mathrm{b}}\mathrm{e}^{\boldsymbol{\Phi}(s)(1-\xi)} & \mathrm{X}<\xi\end{cases}.$$

However, for the free vibration of the SWCNT-based nanomechanical sensor, the right-hand side must vanish. The existence of a non-trivial solution to the corresponding homogenous Eq. (22) indicates that the determinant of the coefficient matrix must vanish.

$$\det\left[\mathbf{M}_{\mathrm{b}}+\mathbf{N}_{\mathrm{b}}\mathrm{e}^{\boldsymbol{\Phi}(s)}+\mathbf{R}_c(s)\mathrm{e}^{\boldsymbol{\Phi}(s)\delta}\right]=0\tag{29}$$

Eq. (29) is the characteristic equation that should be found. Considering the nondimensional natural frequency,

$$\Omega=\sqrt{-\Gamma}=\sqrt{-\frac{\rho AL^4s^2}{EI}}\tag{30}$$

the circular frequency ω of vibration is given by

$$\omega=\mathrm{Im}(s)=\Omega\sqrt{\frac{EI}{\rho AL^4}}\tag{31}$$

where $\mathrm{Im}(s)$ denotes the imaginary part of a complex s. Once the solution of Eq. (29) is found, the natural frequencies

$$f=\frac{\omega}{2\pi}=\frac{\Omega}{2\pi}\sqrt{\frac{EI}{\rho AL^4}}\tag{32}$$

can be directly obtained from Eq. (31). Furthermore, the corresponding modal shapes can be evaluated by

$$\boldsymbol{\eta}(X,s_k)=\mathrm{e}^{\boldsymbol{\Phi}(s_k)X}\boldsymbol{\zeta}_k\tag{33}$$

where s_{k} denotes the imaginary frequency of the nanomechanical sensor for mode k, and ζ_k is a non-trivial vector obtained by substituting s_{k} into the corresponding homogeneous Eq. (28).

3.2 Nonlocal EBT

Similarly, the nondimensional governing equations, boundary conditions, and compatibility conditions for the SWCNT sensor based on nonlocal EBT can be expressed as

$$\frac{\partial^4\tilde{W}(X,s)}{\partial X^4}=\Gamma\lambda^2\frac{\partial^2\tilde{W}(X,s)}{\partial X^2}-\Gamma\tilde{W}(X,s)\tag{34}$$

$$\tilde{W}_1(0,s)=\tilde{W}_2(1,s)=\frac{\partial\tilde{W}_1}{\partial X}(0,s)=\frac{\partial\tilde{W}_2}{\partial X}(1,s)=0\tag{35}$$

$$\tilde{W}_1(\delta,s)=\tilde{W}_2(\delta,s),\ \frac{\partial\tilde{W}_1(\delta,s)}{\partial X}=\frac{\partial\tilde{W}_2(\delta,s)}{\partial X}\tag{36}$$

$$\begin{aligned}&\Gamma\lambda^2\tilde{W}_1(\delta,s)-\frac{\partial^2\tilde{W}_1(\delta,s)}{\partial X^2}-\Gamma\lambda^2\tilde{W}_2(\delta,s)\\&+\frac{\partial^2\tilde{W}_2(\delta,s)}{\partial X^2}=0\end{aligned}\tag{37}$$

$$\begin{aligned}&m\Gamma\tilde{W}_1(\delta,s)+\Gamma\lambda^2\frac{\partial\tilde{W}_1(\delta,s)}{\partial X}-\frac{\partial^3\tilde{W}_1(\delta,s)}{\partial X^3}\\&-\Gamma\lambda^2\frac{\partial\tilde{W}_2(\delta,s)}{\partial X}+\frac{\partial^3\tilde{W}_2(\delta,s)}{\partial X^3}=0.\end{aligned}\tag{38}$$

The TFM is used to solve Eqs. (34) to (38). By introducing the following status vector,

$$\bar{\boldsymbol{\eta}}(X,s)=[\tilde{W}_1,\frac{\partial\tilde{W}_1}{\partial X},\frac{\partial^2\tilde{W}_1}{\partial X^2},\frac{\partial^3\tilde{W}_1}{\partial X^3},\tilde{W}_2,\frac{\partial\tilde{W}_2}{\partial X},\frac{\partial^2\tilde{W}_2}{\partial X^2},\frac{\partial^3\tilde{W}_2}{\partial X^3}]^{\mathrm{T}}$$

a completely analogous procedure can deal with the issue, and the only difference is that the matrices $\bar{\boldsymbol{\Phi}}(s)=[\bar{\Phi}_{ij}]_{8\times8}$, $\bar{\mathbf{M}}_b=[\bar{M}_{ij}]_{8\times8}$, $\bar{\mathbf{N}}_b=[\bar{N}_{ij}]_{8\times8}$, and $\bar{\mathbf{R}}_c=[\bar{R}_{ij}]_{8\times8}$ are still 8×8 matrices, in which $\bar{\Phi}_{12}=\bar{\Phi}_{23}=\bar{\Phi}_{34}=1$, $\bar{\Phi}_{56}=\bar{\Phi}_{67}=\bar{\Phi}_{78}=1$, $\bar{\Phi}_{41}=\bar{\Phi}_{85}=-\Gamma$, $\bar{\Phi}_{43}=\bar{\Phi}_{87}=-\Gamma\lambda^2$, $\bar{M}_{11}=\bar{M}_{22}=1$, $\bar{N}_{35}=\bar{N}_{46}=1$, $\bar{R}_{51}=\bar{R}_{62}=\bar{R}_{77}=\bar{R}_{88}=1$, $\bar{R}_{55}=\bar{R}_{66}=\bar{R}_{73}=\bar{R}_{84}=-1$, $\bar{R}_{71}=\bar{R}_{82}=-\bar{R}_{75}=-\bar{R}_{86}=\Gamma\lambda^2$, $\bar{R}_{81}=m\Gamma$, and other elements in $\bar{\mathbf{M}}_b$, $\bar{\mathbf{N}}_b$, and $\bar{\mathbf{R}}_c$ vanish. Therefore, the characteristic equation based on nonlocal EBT can be expressed as

$$\det\left[\bar{\mathbf{M}}_{\mathbf{b}}+\bar{\mathbf{N}}_{\mathbf{b}}\,\mathrm{e}^{\bar{\boldsymbol{\Phi}}(s)}+\bar{\mathbf{R}}_c\,\mathrm{e}^{\bar{\boldsymbol{\Phi}}(s)\delta}\right]=0.\tag{39}$$

4. Results and discussion

In this section, the effects of the nonlocal parameter, the mass and location of the attached nanoparticle, and the length-to-diameter ratio of the SWCNT on the natural frequencies of a bridged SWCNT are analyzed. The basic parameters used in the calculations for the system are given as follows: Young's modulus $E=1$ TPa, Poisson's ratio $\nu=0.28$, the mass density $\rho=2.3$ g/cm^3, shear correction factor $\kappa=5/6$, the diameter of the SWCNT $d=1.1$ nm, and the effective tube

thickness $t = 0.342$ nm.

4.1 Result validation

Prior to the presentation of numerical results of the natural frequencies, the validity and accuracy of the method should be examined. The absence of the scale parameter, which corresponds to a classical clamped-clamped beam carrying a concentrated mass at the location c measured from the end x=0, should be considered.

The natural frequencies of the SWCNT-based nanomechanical sensor can be computed. The results of the obtained frequencies of a SWCNT with $L/d = 10$ for different values of the mass and positions of the nanoparticle are listed in Table 1 when the nonlocal parameter e_0a/L vanishes. Due to the symmetry of the bridged SWCNT, attention is given to the range of c/L running from 0 to 0.5. For comparison, the commercial FEM software, MSC. Nastran, is used. Using MSC. Nastran, the clamped-clamped beam element defined with a CBEAM entry can account for the effect of shear deformation and rotary inertia, which is justified to model the classical TBT. The corresponding numerical results are also presented in Table 1. Based on Table 1, the theoretical results and the FEM simulation results are in good agreement. For the fundamental frequencies, the maximum relative error is 0.5777%, occurring in the absence of the nanoparticle. Moreover, the relative error becomes less as the attached mass increases or becomes closer to the beam center, which becomes larger for the higher mode. In addition, with the rising mass and location of the attached mass ($0 < c/L \leq 0.5$), the frequencies decrease, indicating the sensitivity of the frequencies of the bridged SWCNT to the attached mass and its position. This scenario embodies the basic principle of SWCNTs as micro-mass detection [8].

4.2 Effect of the attached mass on the SWCNT-based nanomechanical sensor

In this subsection, the frequency shift induced by the attached nanoparticle is analyzed. For this purpose, the frequency shift Δf is defined as the difference between the natural frequencies of a bridged SWCNT with and without the nanoparticle. The frequency shift Δf serves as an index for the quantitative assessment of the mechanical behavior of the nanomechanical sensor.

Fig. 2 shows Δf versus the mass of the nanoparticle m_0 with $L/d = 10$ and $c/L = 0.5$ for mode 1. As pointed out previously, an increase in the mass of the attached nanoparticle gives rise to a decrease in the natural frequencies. In Fig. 2, the frequency shift is also seen to rise as the mass m_0 rises. This phenomenon agrees with that described by Lee et al. [17] and Li et al. [22]. The variation of frequency is apparent when the attached mass is larger than 10 g to 21 g. Thus, the mass sensitivity of the nanomechanical mass sensor can reach at least 10^{-21} g; this range is of the same order mentioned in [22]. Furthermore, due to the size-dependent mechanical properties of SWCNTs, the frequency shift of the nanomechanical sensor becomes smaller if the effect of the nonlocal parameter is taken into account (Fig. 2), which is obvious for larger nanoparticles.

Table 1. Comparison of classical natural frequencies (GHz) obtained from TFM using FEM software for SWCNT sensor with $L/d = 10$ for different values of the attached mass and its position.

m	c/L		f_1	f_3	f_5
0		TFM	229.6831	1005.6764	2018.4681
		FEM	231.0100	1032.0730	2094.2720
		%error	0.5777	2.6248	3.7555
1.0	0.1	TFM	222.5895	700.2197	1719.0650
		FEM	223.7352	712.5485	1781.7040
		%error	0.5147	1.7607	3.6438
	0.3	TFM	145.9764	947.7534	1713.4739
		FEM	146.2825	972.4708	1762.7469
		%error	0.2097	2.6080	2.8756
	0.5	TFM	122.3738	800.1694	1685.0182
		FEM	122.5796	810.0579	1731.6600
		%error	0.1682	1.2358	2.7680
10.0	0.1	TFM	134.8591	646.4289	1702.2854
		FEM	134.9462	658.9860	1764.8920
		%error	0.0646	1.9425	3.6778
	0.3	TFM	55.5184	935.5854	1677.9124
		FEM	55.5345	959.9448	1728.9410
		%error	0.0290	2.6037	3.0412
	0.5	TFM	44.5571	751.5249	1635.9748
		FEM	44.5675	759.3647	1681.8929
		%error	0.0233	1.0432	2.8068

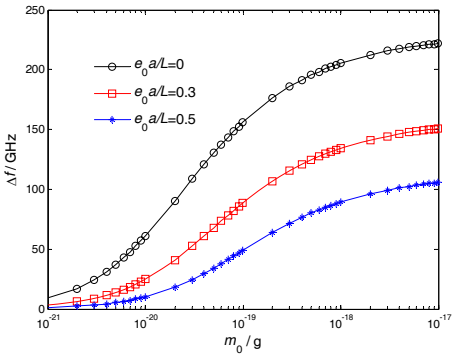

Fig. 2. Small scale effect on the fundamental frequency shift of the SWCNT sensor versus the attached mass with $L/d = 10$ and $c/L = 0.5$.

In addition, the location of the additional nanoparticle can influence the changes in the natural frequency of the SWCNT-based nanomechanical sensor. Fig. 3 illustrates the effect of the location of the nanoparticle, c/L, on the frequency shift of the bridged nanomechanical sensor for $e_0a/L = 0.3$ with $L/d = 10$. The effect of the nanoparticle's location on the frequency shift of the SWCNT sensor is significant. As the nanoparticle nears the beam center, the frequency shift increases. The reason for this may be explained as follows. As shown in Table 1, the frequency of the nanomechanical sensor decreases with the increasing mass of the nanoparticle. Mak-

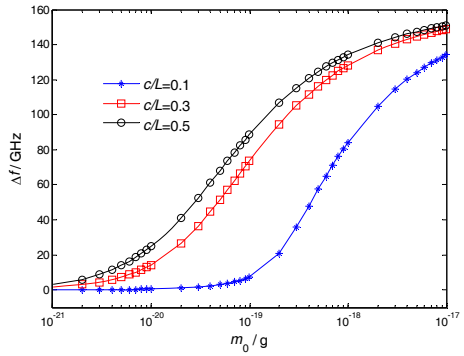

Fig. 3. Location effect of the nanoparticle on the frequency shift of the SWCNT sensor versus the attached mass with $e_0a/L = 0.3$ and $L/d = 10$.

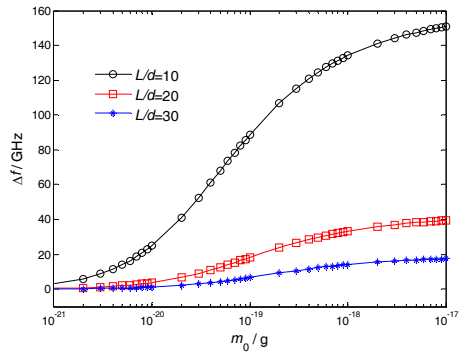

Fig. 4. Effect of the length-to-diameter ratio on the fundamental frequency shift of the SWCNT sensor versus the attached mass with $c/L = 0.5$ and $e_0a/L = 0.3$.

ing the value of c/L closer to the beam center is equivalent to increasing the mass of the nanoparticle at the same location [17]. Therefore, the location of the nanoparticle becomes smaller as its mass increases.

For the TBT, the length-to-diameter ratio or aspect ratio is an important parameter to the natural frequency, which can also influence the change in the frequency of the nanomechanical sensor. Fig. 4 depicts the effect of the length-to-diameter ratio of the SWCNT, L/d, on the frequency shift of the nanomechanical sensor with $c/L = 0.5$ for $e_0a/L = 0.3$ and mode 1. The effect of the length-to-diameter ratio on the natural frequencies is significant. The frequency shift becomes larger when the length-to-diameter ration is small, especially when the attached mass is larger. Thus, mass sensitivity increases when smaller SWCNT resonators are used in mass sensors. This result is in agreement with the previous study for CNT-based nanomechanical resonators [22]. The length-to-diameter ratio mainly affects the stiffness of the SWCNT, whereas the attached mass increases the total mass of the system. Thus, increasing the value of the length-to-diameter ratio is equivalent to increasing the mass of the nanoparticle.

4.3 Effect of shear deformation and rotary inertia on the SWCNT-based nanomechanical sensor

The difference between the results of the natural frequencies while adopting the nonlocal EBT and TBT is compared. The former neglects shear deformation and rotary inertia. For simplicity, the attached nanoparticle is assumed to be equal to the mass of the SWCNT. A comparison of the frequency ratio f_{NT}/f_{NE} is demonstrated in Fig. 5, with the length-to-diameter ratio for $c/L = 0.5$, $e_0a/L = 0.3$, and $m = 1$. Here, the subscripts NT and NE represent the nonlocal TBT and EBT. As shown in Fig. 5, the values of f_{NT}/f_{NE} are always smaller than unity for all modes, indicating that the frequencies based on the nonlocal EBT are overestimated, particularly for higher-order frequencies, as those in the classical theory. In other words, the nonlocal TBT is more adequate than the nonlocal EBT for its consideration of shear deformation and rotary inertia. This conclusion is especially evident for short SWCNT-based nanomechanical sensors. However, for slender SWCNT-based nanomechanical sensors, the frequency from the nonlocal EBT still yields sufficiently accurate results, which may be attributed to the essential drawback of the Euler-Bernoulli hypothesis, irrespective of the nonlocal and classical models. Therefore, for a short SWCNT-based nanomechanical sensor, the TBT should be employed instead of the EBT.

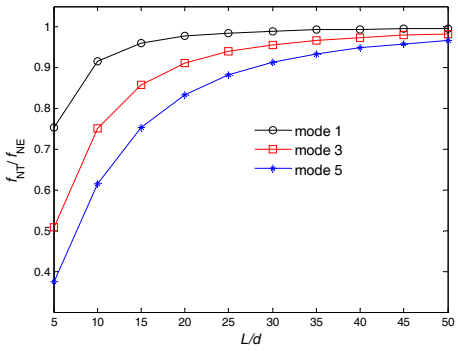

Fig. 5. Effects of transverse shear deformation and rotary inertia on vibration frequencies for SWCNT-based nanomechanical mass sensor with $m = 1$, $c/L = 0.5$, and $e_0a/L = 0.3$.

5. Conclusions

In this paper, the frequency shift of an SWCNT-based nanomechanical mass sensor was investigated. Using the nonlocal TBT, the governing equation of a clamped SWCNT carrying a nanoparticle at any position was derived, and the natural frequencies were determined by the TFM. The results of this study were confirmed by the results using the FEM. The conclusions are as follows:

- Increasing the mass of the nanoparticle or making it closer to the beam center decreases the natural frequencies, but increases the frequency shift.
- The frequency shift of the SWCNT-based nanomechanical mass sensor becomes smaller when the effect of the nonlocal parameter is taken into account.
- The frequency shift of the SWCNT-based nanomechanical sensor is more sensitive for small length-to-diameter ratios of the SWCNT, especially when a larger nanoparti-

cle is carried.

- The nonlocal TBT, which takes into account shear deformation and rotary inertia, is more adequate than the nonlocal EBT.

Acknowledgment

We would like to thank the excellent postgraduate innovation project of the National University of Defense Technology (B100103) and Hunan Provincial Innovation Foundation For Postgraduate (CX2010B001) for the support of this work. We gratefully acknowledge Professor Xian-Fang Li of Central South University, China for the helpful discussions. We also thank three anonymous reviewers for giving helpful suggestions to improve the original manuscript.

References

[1] S. Iijima, Helical microtubules of graphitic carbon, *Nature,* 354 (1991) 56-58.

[2] S. Lu, C. Cho, K. Choi, W. Choi, S. Lee and N. Wang, An inscribed surface model for the elastic properties of armchair carbon nanotube, *J. Mech. Sci. Technol.,* 24 (2011) 2233-2239.

[3] H. J. Dai, J. H. Hafner, A. G. Rinzler, D. T. Colbert and R. E. Smalley, Nanotubes as nanoprobes in scanning probe microscopy, *Nature,* 384 (1996) 147-150.

[4] P. Kim and C. M. Lieber, Nanotube nanotweezers, *Science,* 286 (1999) 2148-2150.

[5] Q. Zheng and Q. Jiang, Multiwalled carbon nanotubes as gigahertz oscillators, *Phys. Rev. Lett.,* 88 (2002) 045503.

[6] P. Poncharal, Z. L. Wang, D. Ugarte and W. A. D. Heer, Electrostatic deflections and electro-mechanical resonances of carbon nanotubes, *Science,* 283 (1999) 1513-1516.

[7] K. Jensen, K. Kim and A. Zettl, An atomic-resolution nanomechanical mass sensor, *Nat. Nanotechnol,* 3 (2008) 533-537.

[8] R. Chowdhury, S. Adhikari and J. Mitchell, Vibrating carbon nanotube based bio-sensors, *Physica E,* 42 (2009) 104-109.

[9] I. Mehdipour, A. Barari and G. Domairry, Application of a cantilevered SWCNT with mass at the tip as a nanomechanical sensor, *Comput. Mater. Sci.,* 50 (2011) 1830-1833.

[10] D. H. Wu, W. T. Chien, C. S. Chen and H. H. Chen, Resonant frequency analysis of fixed-free single-walled carbon nanotube-based mass sensor, *Sens. Actuators, A,* 126 (2006) 117-121.

[11] S. Timoshenko, On the correction for shear of the differential equation for transverse vibrations of prismatic bars, *Philos. Mag.,* 41 (1921) 744-746.

[12] X. F. Li and B. L. Wang, Vibrational modes of Timoshenko beams at small scales, *Applied Physics Letters,* 94 (2009) 101903.

[13] C. M. Wang, Y. Y. Zhang, S. S. Ramesh and S. Kitipornchai, Buckling analysis of micro- and nano-rods/tubes based on nonlocal Timoshenko beam theory, *J. Phys. D: Appl. Phys.,* 39 (2006) 3904-3909.

[14] Y. Yang, L. X. Zhang and C. W. Lim, Wave propagation in double-walled carbon nanotubes on a novel analytically nonlocal Timoshenko-beam model, *J. Sound Vib.,* 330 (2011) 1704-1717.

[15] A. C. Eringen, On differential equations of nonlocal elasticity and solution of screw dislocation and surface waves, *J. Appl. Phys.,* 54 (1983) 4703-4710.

[16] A. C. Eringen, *Nonlocal continuum field theories*, Springer, New York (2002).

[17] H. L. Lee, J. C. Hsu and W. J. Chang, Frequency shift of carbon-nanotube-based mass sensor using nonlocal elasticity theory, *Nanoscale Res. Lett.,* 5 (2010) 1774-1778.

[18] B. Yang, Transfer function of constrained/combined one-dimensional continuous dynamic systems, *Journal of Sound and Vibration,* 156 (1992) 425-443.

[19] B. Yang and C. A. Tan, Transfer function of one-dimension distributed parameter system, *Journal of Applied Mechanics,* 59 (1992) 1009-1014.

[20] J. P. Zhou and B. Yang, A distributed transfer function method for analysis of cylindrical shells, *AIAA J.,* 33 (1995) 1698-1708.

[21] M. Aydogdu and S. Filiz, Modeling carbon nanotube-based mass sensors using axial vibration and nonlocal elasticity, *Physica E,* 43 (2011) 1229-1234.

[22] C. Y. Li and T. W. Chou, Mass detection using carbon nanotube-based nanomechanical resonators, *Appl. Phys. Lett.,* 84 (2004) 5246-5248.

[23] H. Y. Chiu, P. Hung, H. W. C. Postma and M. Bockrath, Atomic-scale mass sensing using carbon nanotube resonators, *Nano Lett.,* 8 (2008) 4342-4346.

[24] S. Cuenot, C. Frétigny, S. Demoustier-Champagne and B. Nysten, Measurement of elastic modulus of nanotubes by resonant contact atomic force microscopy, *J. Appl. Phys.,* 93 (2003) 5650-5655.

[25] C. M. Wang, Y. Y. Zhang and X. Q. He, Vibration of nonlocal Timoshenko beams, *Nanotechnology,* 18 (2007) 105401.

[26] S. Adhikari, M. I. Friswell and Y. Lei, Modal analysis of nonviscously damped beams, *ASME J. Appl. Mech.,* 74 (2007) 1026-1030.

Zhi-Bin Shen received his B.S. degree from National University of Defense Technology (NUDT) in Changsha, China in 2006. Mr. Shen is currently a Ph.D candidate at the College of Aerospace and Materials Engineering, NUDT. His research interests include vibration analyses of carbon nanotubes and graphene sheets.

Guo-Jin Tang received his Ph.D degree in solid mechanics at NUDT, China in 1998. Dr. Tang is currently a professor in the College of Aerospace and Materials Engineering at NUDT. His research interests include computational solid mechanics and spacecraft dynamics and control.